Analysis of the Quadrupolar Coupling Effect on the Line Intensities Using Single-Crystal Nutation NMR in α-Al$_2$O$_3$ Crystals

Ae Ja Woo,[*] Duk-Young Han,[†] and So Hyun Cho

Department of Science Education, Ewha Womans University, Seoul 120-750, Korea
[†]Korea Basic Science Institute, Seoul 136-701, Korea
Received June 18, 1999

With 1D-nutation NMR for a spin I = 5/2 system, the relative line intensities of the central and the inner- and outer-satellite transitions are calculated as functions of quadrupolar coupling ω_Q and rf pulse strength ω_{rf}. Experimentally measured line intensities including both central and satellites are used to extract the values of ω_Q and ω_{rf} from nonlinear least-squares fits. The method is illustrated in α-Al$_2$O$_3$ crystals (ruby and corundum) with the single-crystal ^{27}Al nutation NMR spectra. As a result, the new feature that the rf pulse strength shows reduced effect on the satellite transition lines according to the quadrupolar coupling is discussed by using a fictitious spin-1/2 operator.

Introduction

Solid-state ^{27}Al (I = 5/2) NMR spectroscopy has been widely used to investigate the inorganic solids such as zeolites, glasses, ceramics, and clay minerals. The ^{27}Al NMR quadrupolar coupling, which describes the principal elements of the electric field gradient tensor, depends on the local symmetry around the nucleus and gives direct structural information. For a powdered material, MAS (magic angle spinning),[1,2] VAS (variable angle spinning),[3] DAS (dynamic angle spinning),[4,5] DOR (double rotation),[6,7] and MQ (Multiple Quantum) MAS[8,9] NMR have been applied for determining quadrupolar coupling constant e^{2}qQ/h and asymmetry parameter η by acquiring high-resolution spectra. Single-crystal NMR[10,11] also provides the most direct approach to determine the quadrupolar coupling parameters. In these NMR techniques, the effect of quadrupolar interaction during rf pulse excitation is completely ignored assuming it is much weaker than the excitation pulse, which is not easy to be the case in real experiments. On the other hand, in the nutation NMR technique, the spin dynamics nutating around rf magnetic field under the influence of the stronger quadrupolar interaction during pulsing can be observed.

For half-integer quadrupolar spin systems, 1D- and 2D-nutation NMR are effective techniques to determine the quadrupolar coupling parameters and to resolve the overlapping powder patterns with dissimilar quadrupolar interactions, respectively. For a spin I = 5/2 system, extensive works have been done theoretically and also experimentally. A. P. M. Kentgen, W. S. Veeman, and P. P. Man have given theoretical descriptions of 1D- and 2D-nutation NMR.[12-15] The ^{27}Al 1D-nutation NMR has been used to determine the quadrupolar coupling in a corundum (α-Al$_2$O$_3$) crystal.[12] Applications of the ^{27}Al 2D-nutation NMR on the structural studies of inorganic solids[16-18] present successful results. All of these works focused only on the analysis of the central line intensities.

Herein, we are trying to determine the ^{27}Al NMR quadrupolar coupling in α-Al$_2$O$_3$ crystals from the relative line intensities of the central and the inner- and outer-satellite transitions in the 1D-nutation NMR spectra. In this course, we expect two distinctive features: (1) The modulation pattern of central transition is affected by the satellite transitions. (2) The rf pulse strength over the satellite transitions is reduced compared to that over the central transition.

Theory

Scheme 1 shows a graphical description for the x-nutation NMR pulse sequence.

$H_{rf} + H_Q^{(1)}$

X

t_1 t_2
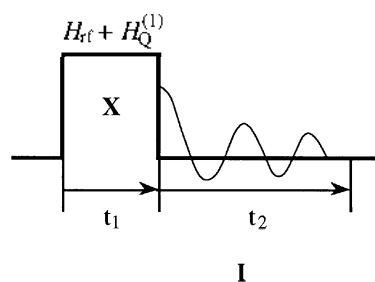
I

For a spin I = 5/2 system, the Hamiltonian during rf pulse excitation in the rotating frame is represented by

$$H_{on} = H_{rf} + H_Q^{(1)} = -\omega_{rf}I_x + \frac{1}{3}\omega_Q(3I_z^2 - I(I+1))$$

$$\omega_Q = \frac{3}{80}\frac{e^2qQ}{h}(3\cos^2\theta - 1 + \eta\sin^2\theta\cos^2\phi) \qquad (1)$$

where H_{rf} and $H_Q^{(1)}$ represent the coupling of the spin with the rf magnetic field and the first order quadrupolar interaction, respectively. θ and ϕ are Euler angles needed to orient the principal axis of electric field gradient tensor with respect to the applied magnetic field.

The spin dynamics excited by a x-nutation pulse can be described by the density matrix. The evolution of density matrix during t_1 is obtained by solving the Liouville-von Neumann equation as follows;

$$\rho(t_1)_{ij} = \{\exp(-iH_{on}t_1)\rho(0)\exp(iH_{on}t_1)\}_{ij}$$

$$- \{ T\exp(-iT^- H_{on} Tt_1) T^+ \rho(0) T\exp(iT^+ H_{on} Tt_1) T^+ \}_{ij}$$

$$- \sum_{k,l} \{ T_{ik} T_{jl}^+ \exp\{-i\Omega_{kl} t_1\} \} (T^- \rho(0) T)_{kl} \} \tag{2}$$

where $\Omega_{kl} = (E_k - E_l)$, represents nine nutation frequencies as shown in Scheme II, which only depend on the eigenvalues.
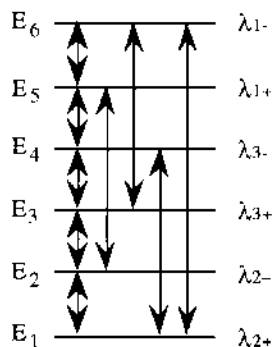
II

Unitary matrix (T) diagonalizing Hamiltonian H_{on} can be found by solving the eigenvalue equation and its secular equation like

$$H_{on} \Psi_i - \lambda_i \Psi_i \text{ and } \text{Det}(H_{on} - \lambda I) - 0. \tag{3}$$

The equilibrium density matrix $\rho(0)$ corresponds to I_z and $T^+ \rho(0) T$ is expressed by

$$T^\dagger \rho(0) T = \begin{bmatrix} 0 & 0 & 0 & S_{11} & S_{12} & S_{13} \\ 0 & 0 & 0 & S_{21} & S_{22} & S_{23} \\ 0 & 0 & 0 & S_{31} & S_{32} & S_{33} \\ S_{11} & S_{21} & S_{31} & 0 & 0 & 0 \\ S_{12} & S_{22} & S_{32} & 0 & 0 & 0 \\ S_{13} & S_{23} & S_{33} & 0 & 0 & 0 \end{bmatrix}. \tag{4}$$

And, the line intensity of the central $(S(t_1)_{34})$ and inner- $(S(t_1)_{23})$ and outer- $(S(t_1)_{12})$ satellite transitions during t_1 are represented as

$$S(t_1)_{ij} = [\rho(t_1)_{ji}(I_x)_{ij}]$$

$$\text{Thus, } S(t_1)_{34} = 3\rho(t_1)_{43} = \frac{3}{2} i \sum_i^3 \sum_{i,j}^3 S_{ij} Z_{i-} Z_{j-} \sin(\lambda_{ij} t_1)$$

$$S(t_1)_{23} = 2\sqrt{2} \rho(t_1)_{32} = \frac{\sqrt{2}}{2} \sum_i^3 \sum_{i,j}^3$$

$$S_{ij} \{ i(Y_{j-} Z_{j-} - Y_{j-} Z_{ij}) \} \sin(\lambda_{ij} t_1)$$

$$S(t_1)_{12} = \sqrt{5} \rho(t_1)_{21} = \frac{\sqrt{5}}{4} \sum_i^3 \sum_{i,j}^3$$

$$S_{ij} \{ i(X_{ii} Y_{j-} - X_{j-} Y_{i-}) \} \sin(\lambda_{ij} t_1). \tag{5}$$

where $S_{ij} - 5X_{i+}X_{j-} + 3Y_{i+}Y_{j-} \cdot Z_{i+}Z_{j-}$ and $\lambda_{ij} - \lambda_{i-}-\lambda_{j-}$. The terms $X_{i+}, X_{j-}, Y_{i+}, Y_{j-}, Z_{i-},$ and Z_{j-} are described in details in

the reference.[19] Eqn. (5) shows that each line intensity is the sum of nine sine curves of different amplitudes and frequencies. And the relative line intensities of the central and satellite transition depend on the values of ω_Q and ω_{rf}.

Experimental Section

^{27}Al nutation NMR spectra were acquired on a Bruker MSL200 solid-state NMR spectrometer operating at 52.2 MHz. α-Al$_2$O$_3$ crystals (ruby and corundum) were mounted on a high-power wideline probe and oriented by a goniometer. The x-nutation pulse sequence was applied. The rf pulse length t_1 was incremented in steps of 1 μs from 0 μs. The rf pulse strengthes ω_{rf} were adjusted to 25 kHz and 63 kHz which correspond to 90° pulse lengthes of 10 μs and 4 μs, respectively, for corundum and ruby. An aqueous solution of Al(H$_2$O)$_6$[31] was used to determine 90° pulse length. A relaxation delay of 20 s and a dead time of 8 μs were used. Each spectrum was obtained by summing 10 free induction decays. Exponential line broadening of 800 Hz and no zero filling were applied. The relative line intensities of central and satellite transitions were measured from a Fourier-transformed and manually-phased spectrum.

Results and Discussion

Shown in Figure 1(a) is the ^{27}Al single-crystal nutation NMR spectra for a corundum crystal at a fixed orientation with respect to the applied magnetic field. Signal-to-noise ratio (S/N~50) of the central transition line for $t_1 - 1$ μs is enough to measure the line intensity with high accuracy. Because of the large spectral width (2.5 MHz), only the central transition line was properly phased in a spectrum. All spectra were drawn on the absolute intensity scale. The relative line intensities of inner- and outer-satellite transitions were obtained by averaging each pair of the satellites. In Figure 1(b), we show the experimental symmetrized stick spectra recreated from the relative line intensities of the ^{27}Al nutation NMR spectra. From the line separation between inner-satellite transitions, theoretically four times of quadru-
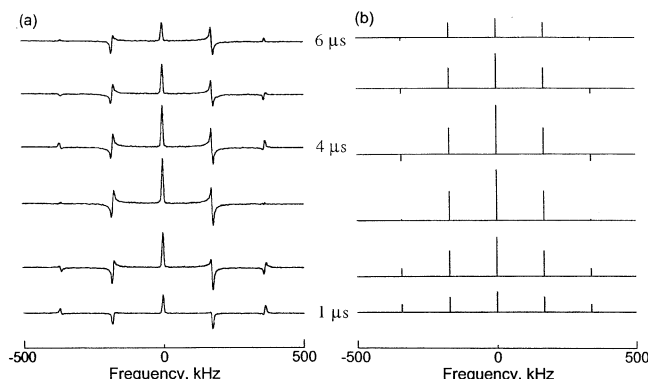

Figure 1. (a) Experimental ^{27}Al nutation NMR spectra of a corundum crystal at a fixed orientation for rf pulse length $t_1 = 1$ to 6 μs. (b) Experimental symmeterized stick spectra recreated from the relative line intensities of the ^{27}Al nutation NMR spectra.
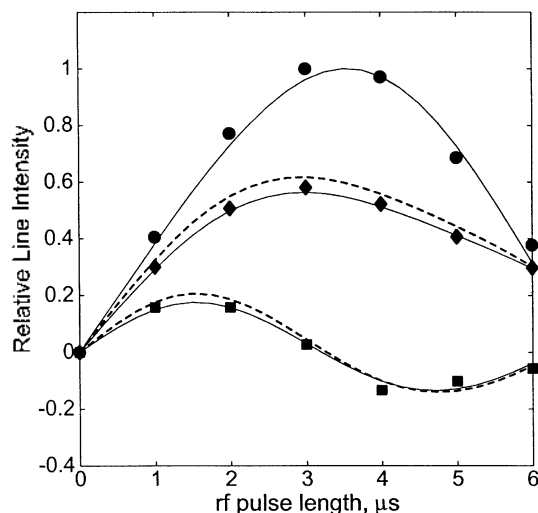
Figure 2. Results from nonlinear least-squares analysis of the relative line intensities of the central and inner- and outer-satellite transitions measured from Figure 1. Experimental data are represented as circles (●) and diamonds (◆) and squares (■) for the central and the inner- and outer-satellite transitions, respectively. The solid lines (—) were calculated with the best fitted parameters. The dashed lines (---) were obtained without the effect of the reduced rf pulse strength over the satellite transitions.

Table 1. Results of Nonlinear Least-Squares Fits to the Single-Crystal ^{27}Al Nutation NMR Spectra of α-Al$_2$O$_3$ Crystals

	ω_Q (kHz)	ω_{rf} (kHz)	α	β
Corundum	81.2(6)	67.2(5)	0.89(7)	0.84(2)
Ruby I[a]	26.7(7)	19.6(6)	0.71(9)	0.39(2)
II[b]	62.9(2)	19.6(6)	0.84(2)	0.35(4)
III[c]	77.6(2)	19.6(6)	0.86(7)	0.46(4)

[a]corresponds to Figures 3(a), 4(a), and 5(a). [b]corresponds to Figures 3(b), 4(b), and 5(b). [c]corresponds to Figures 3(c), 4(c), and 5(c).
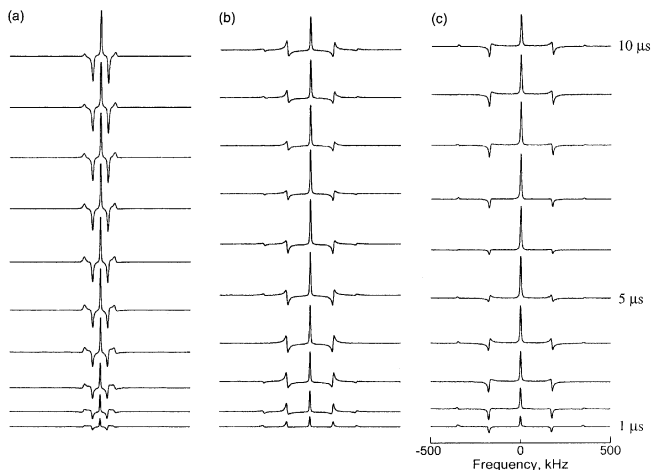

Figure 3. Experimental ^{27}Al nutation NMR spectra of a ruby crystal at three orientations for rf pulse length $t_1 = 1$ to $10\ \mu s$. Three orientations I, II, and III correspond to figure (a), (b), and (c), respectively.

polar coupling (−4ω_Q), ^{27}Al NMR quadrupolar coupling with axial symmetry in a corundum crystal were experimentally determined to be ~85 kHz.

Figure 2 shows the nonlinear least-squares fits to the relative line intensities of the central and the inner- and outer-satellite transitions measured from Figure 1. Experimental data are represented as circles (●) and diamonds (◆) and squares (■) for the central and the inner- and outer-satellite transitions, respectively. The best calculated fits are represented as the solid lines (—) and the calculations are done by using Eqn. (5). The Levenberg-Marquardt nonlinear least-squares algorithm[20] was used. The important fitted parameters are ω_Q and ω_{rf}. In order to correct the systematic experimental errors such as rf pulse rising time, probe frequency response effect, and finite rf pulse effect, imperfections in t_1 and ω_{rf} are also considered. Finally, variable contribution factors α and β are also included in Eqn. (7), which have an effect on the line intensities of the inner- and outer-satellite transitions, respectively. Fitted parameters for the corundum crystal are listed in Table 1.

Figure 3 shows the ^{27}Al nutation NMR spectra for a ruby crystal at three orientations (I, II, and III) with respect to the applied magnetic field at a constant rf field strength. Figures 3(a), 3(b), and 3(c) correspond to the orientations I, II, and III. These orientations were purposely chosen to show the spectra of the different quadrupolar interaction. ^{27}Al NMR quadrupolar couplings with axial symmetry were experimentally determined to be ~25, ~67, and ~83 kHz, respectively, for three orientations. Figure 4 represents the nonlinear least-squares fits to the experimental line intensities of the central and the inner-satellite transitions. Experimental data are represented as circles (●) and diamonds

(◆) and squares (■) for the central and the inner- and outer-satellite transitions, respectively. The best calculated fits are represented as the solid lines (—). Fitted parameters for a ruby crystal are also listed in Table 1. The values of ω_Q and ω_{rf} extracted from nonlinear least-squares fits are in good agreement with those determined from the experimental data.

There is an interesting feature investigated in this work: the line intensities of the satellite transitions relative to the central transition are affected by the reduced rf pulse strength. In case the effect of the reduced rf pulse strength over the satellite transitions is not considered, the relative line intensities of the inner- and outer-satellite transitions are represented as the dashed lines (---) shown in Figures 2 and 4. It could be explained in terms of the fictitious spin-1/2 operator. Hamiltonian for the rf pulse excitation $\omega_{rf}I_x$ can be expressed like

$$\omega_{rf}I_x = \omega_{rf}(\beta\sqrt{5}I_x^{12} + \alpha 2\sqrt{2}I_x^{23} + 3I_x^{34} + \alpha 2\sqrt{2}I_x^{45} + \beta\sqrt{5}I_x^{56})$$

$$(7)$$

The additional factors α and β should be considered because the rf pulse strength over the inner- and outer-satellite transitions can be reduced in reality. Ideally, the values of α and β are equal to 1 in the nutation NMR theory.[21,22] The values of α and β extracted from the nonlinear least-squares fit for α-Al$_2$O$_3$ crystals are listed in Table 1. Moreover, it is quite
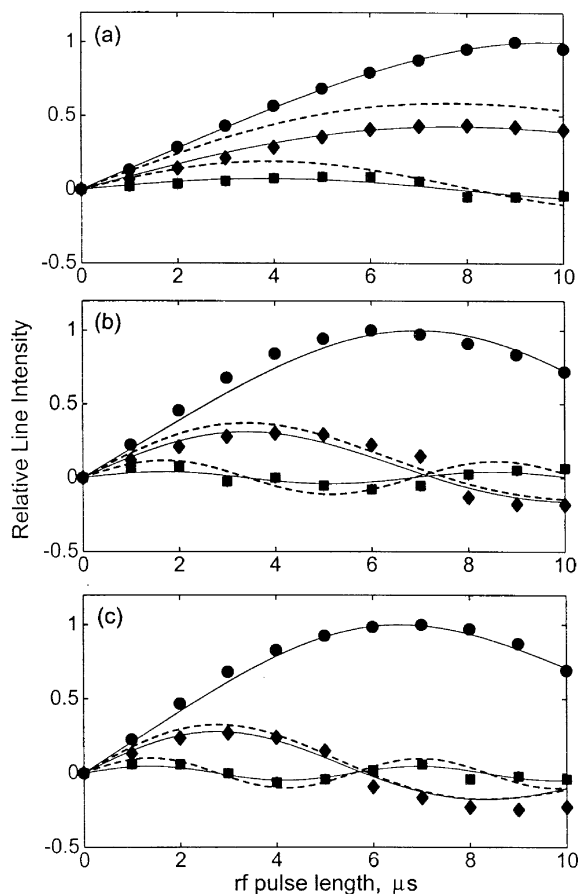
Figure 4. Results from nonlinear least-squares analysis of the relative line intensities of the central and inner-satellite transitions measured from Figure 3. Experimental data are represented as circles (●) and diamonds (◆) and squares (■) for the central and the inner- and outer-satellite transitions, respectively.. The solid lines (——) are calculated with the best fitted parameters. The dashed lines (---) were obtained without the effect of the reduced rf pulse strength over the satellite transitions.

interesting to show the relationship between the values of ω_Q and α and β. However, at this moment, it is difficult to quantitatively explain the trends of the factors α and β correlated with the values of ω_Q and ω_{rf}.

Figure 5 shows the simulated single-crystal ^{27}Al nutation spectra for $t_1 - 0$ to 31 μs, which are calculated by using the same set of the fitted parameters as extracted from nonlinear least-squares fittings. As shown in Figure 5, the nutation of the quadrupolar nuclei are represented as functions of the quadrupolar coupling and the rf pulse strength. The amplitude and frequency modulation clearly shows that there exists the mutual relation between the central and the satellite transitions.

Conclusions

^{27}Al NMR quadrupolar couplings in α-Al$_2$O$_3$ crystals (corundum and ruby) were determined from the analysis of the single-crystal ^{27}Al nutation NMR spectra. The experimentally measured relative line intensities of the central and
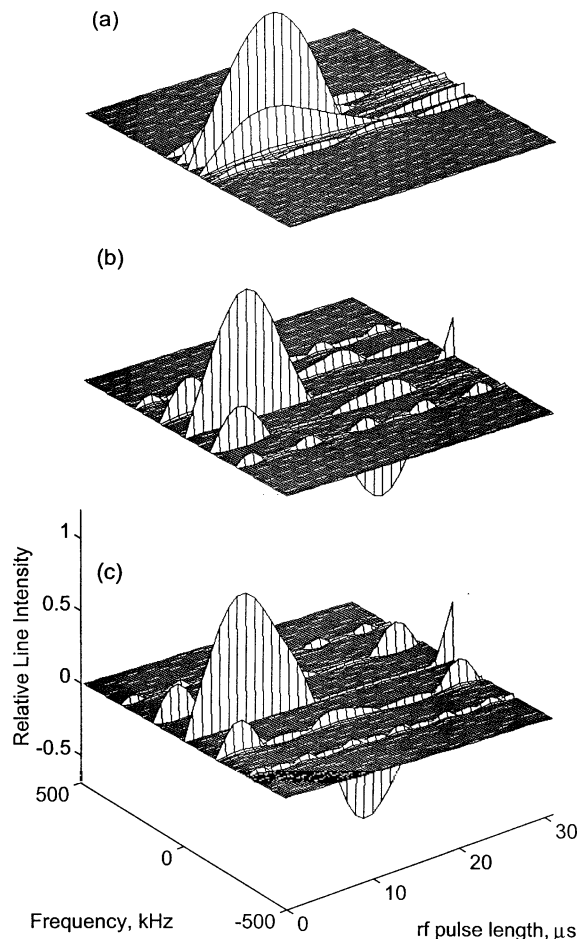

Figure 5. Simulated 1D-nutation spectra for a spin I = 5/2 system, which are calculated using the same values of the fitted parameters for a ruby crystal at three orientations as listed in Table 1.

the inner- and outer-satellite transitions were used for the nonlinear least-squares fitting. In the course of this work, we found that the rf pulse strength according to the quadrupolar coupling has an reduced influence on the line intensities of the satellite transitions. As a result, the analysis of the satellite transitions is necessary for the correct understanding of the central transition.

References

1. Skibsted, J.; Vosegaard, T.; Bildsoe, H.; Jakobsen, H. J. *J. Phys. Chem.* **1996**, *100*, 14872.
2. Kloprogge, J. T.; Dirken, P. J.; Jansen, J. B. H.; Geus, J. W. *J. Non-Cryst. Solids* **1995**, *181*, 151.
3. Sepa, J.; Gorte, R. J.; White, D.; Kassab, E.; Allavena, M. *Chem. Phys. Lett.* **1996**, *262*, 321.
4. Wang, S. H.; Xu, Z.; Baltisberger, J. H.; Bull, L. M.; Stebbins, J. F.; Pines, A. *Solid State Nucl. Magn. Reson.* **1997**, *8*, 1.

5. Grandinetti, P. J.; Baltisberger, J. H.; Farnan, I.; Stebbins, J. F.; Werner, U.; Pines, A. *J. Phys. Chem.* **1995**, *99*, 12341.

6. Kovalakova, M.; Grobet, P. J. *Solid State Nucl. Magn. Reson.* **1997**, *9*, 107.

7. Engelhardt, G. *Microporous Mater.* **1997**, *12*, 369.

8. Woo, G.; Rovnyak, D.; Griffin, R. G. *J. Am. Chem. Soc.* **1996**, *118*, 9326.

9. Brown, S. P.; Wimperis, S. *J. Magn. Reson.* **1997**, *128*, 42.

10. Eichele, K.; Chan, J. C. C.; Washlishen, R. E.; Britten, J. F. *J. Phys. Chem. A* **1997**, *101*, 5423.

11. Vosegaard, T.; Massiot, D.; Gautier, N.; Jakobsen, H. J. *Inorg. Chem.* **1997**, *36*, 2446.

12. Man, P. P. *Molec. Phys.* **1993**, *78*, 307.

13. Van Der Mijden, J. A. M.; Janssen, R.; Veeman, W. S. *Molec. Phys.* **1990**, *69*, 53.

14. Samoson, A.; Lippmaa, E. *J. Magn. Reson.* **1988**, *79*, 255.

15. Kentgens, A. P. M.; Lemmens, J. J. M.; Geurts, F. M. M.; Veeman, W. S. *J. Magn. Reson.* **1987**, *71*, 62.

16. Yano, T.; Mizuno, J.; Shibata, S.; Yamane, M.; Inoue, S.; Onoda, Y. *J. Non-Cryst. Solids* **1997**, *213*, 345.

17. Man, P. P.; Klinowski, J. *Chem. Phys. Lett.* **1988**, *147*, 581.

18. Geurts, F. M. M.; Kentgens, A. P. M.; Veeman, W. S. *Chem. Phys. Lett.* **1985**, *120*, 206.

19. Cho, S. H. *MS Thesis*; Ewha Womans University: Seoul, 1997.

20. Kim, A. J.; Butler, L. G. *Concepts Magn. Res.* **1992**, *4*, 205.

21. Wokaun, A.; Ernst, R. R. *J. Chem. Phys.* **1977**, *67*, 1752.

22. Vega, S. *J. Chem. Phys.* **1978**, *68*, 5518.